

Berry Phase of Dirac Nodal Line Semimetal in Single-Component Molecular Conductor

Yoshikazu Suzumura*, and Ai Yamakage

Department of Physics, Nagoya University, Chikusa-ku, Nagoya 464-8602, Japan

(Received)

The Berry phase and curvature are studied for the Dirac nodal line semimetal of single-component molecular conductor [Pd(dddtt)₂]. Using two-band model on the basis of a tight-binding model, it is shown that the Berry curvature, $\mathbf{B}(\mathbf{k})$, exists along a loop of the nodal line, on which the Berry phase is obtained from surface integral of $\mathbf{B}(\mathbf{k})$. The Berry phase, which is called Zak phase, is also calculated from one-dimensional integral of the Berry connection along a line between two equivalent points of boundaries of Brillouin zone. The possible experiment is discussed in terms of the Berry phase.

It has been known that Dirac electrons appear in condensed matter when two neighboring bands such as the conduction and valence bands degenerate at a crystal momentum.¹⁾ The Dirac fermion which originally was found in the massive relativistic particle is realized in graphite as the massless Dirac electron, which obeys the Weyl equation.²⁾ Since the discovery of such electron in graphene monolayer,³⁾ several properties of two-dimensional Dirac electrons have been studied extensively. The Dirac electrons, which exist as the bulk system and are located close to chemical potential, have been found in organic conductor⁴⁾ α -(BEDT-TTF)₂I₃ and single-component molecular conductor⁵⁾ [Pd(dddtt)₂] where the former shows two-dimensional Dirac electrons and the latter shows three-dimensional Dirac electrons with Dirac nodal line semimetal.⁶⁾ Such nodal line has been studied due to unconventional loop of the Dirac points.^{7–13)} The noticeable phenomena of Dirac electrons come from topological property of wavefunction, which is known as the Berry phase.¹⁴⁾ Such topological property is fundamental for the Hall conductivity,³⁾ in addition to the energy dispersion of the Dirac cone, which takes a crucial role for the almost temperature-independent conductivity.¹⁵⁾

The present paper focuses on the Dirac electrons in the molecular conductor, which are most promising candidate to observe these properties due to chemical potential located close to the nodal line. Although the Berry phase¹⁴⁾ for the Dirac point of α -(BEDT-TTF)₂I₃ was shown explicitly,¹⁶⁾ that of [Pd(dddtt)₂] is not yet clarified due to non-coplanar three-dimensional loop. Thus, we calculate the Berry curvature in [Pd(dddtt)₂] using a reduced Hamiltonian of two-band model, which is similar to that of CaAgX.⁹⁾

We consider a Dirac electron system consisting of M molecular sites per unit cell, $M = 8$ for [Pd(dddtt)₂].⁶⁾ The Schrödinger equation is given by

$$H(\mathbf{k})|n(\mathbf{k})\rangle = E_n|n(\mathbf{k})\rangle, \quad (1)$$

where $\mathbf{k} = (k_x, k_y, k_z)$ is a three-dimensional wave vec-

tor with a lattice constant taken as unity, and $n (= 1, 2, \dots, M)$ denotes a band index. Quantities $H(\mathbf{k})$, $E_n(\mathbf{k})$ and $|n(\mathbf{k})\rangle$ are the $M \times M$ matrix Hamiltonian with the base of 8 molecular orbitals, eigenvalue (band energy) and eigenfunction (wavefunction), respectively. The nodal line in the present system exists between $E_4(\mathbf{k})$ and $E_5(\mathbf{k})$, which are the conduction and valence bands due to a half-filled band.

The Berry phase γ_n is given by¹⁴⁾

$$\gamma_n = i \int_C d\mathbf{k} \cdot \langle n(\mathbf{k}) | \nabla_{\mathbf{k}} | n(\mathbf{k}) \rangle = \int_S \mathbf{B}_n(\mathbf{k}) \cdot d\mathbf{S}, \quad (2a)$$

$$\mathbf{B}_n(\mathbf{k}) = -\text{Im}\{(\nabla_{\mathbf{k}} \langle n(\mathbf{k}) |) \times \nabla_{\mathbf{k}} | n(\mathbf{k}) \rangle\}, \quad (2b)$$

where $\langle n(\mathbf{k}) | \nabla_{\mathbf{k}} | n(\mathbf{k}) \rangle$ and $\mathbf{B}_n(\mathbf{k})$ denote the Berry connection and curvature, respectively. C denotes a closed path and S is the area enclosed by the path.

We examine \mathbf{B} and γ , which denote $\mathbf{B}_4(\mathbf{k})$ and γ_4 , respectively, for the conduction band. As shown later, the Dirac nodal line is understood by γ , which is a scalar quantity given by $\pm\pi$ or zero, but depends on \mathbf{k} related to the path C . Since $\mathbf{B}(\mathbf{k})$ is essentially determined by E_4 and E_5 , Eq. (2b) is calculated by introducing a 2×2 reduced Hamiltonian $H^{\text{red}}(\mathbf{k})$ relevant to these two bands. The Hamiltonian H is rewritten as $H = H_0 + H_1$, where H_0 consists of two kinds of electrons with different parity and H_1 denotes the interaction between them. Reduced Hamiltonian, $H^{\text{red}}(\mathbf{k})$, has matrix elements ($i=1,2$ and $j=1,2$) given by

$$\begin{aligned} H^{\text{red}}(\mathbf{k})_{ij} &= h_{ij} \\ &= \langle \bar{i} | (H_0(\mathbf{k}) + H_1(\mathbf{k}) - H_0(\mathbf{G}/2)) | \bar{j} \rangle, \end{aligned} \quad (3)$$

where $|\bar{1}\rangle$ and $|\bar{2}\rangle$ are eigenfunctions of the conduction and valence bands at a TRIM (time reversal invariant momentum) $\mathbf{k} = \mathbf{G}/2$ and are calculated from $H_0(\mathbf{G}/2)|\bar{1}\rangle = \bar{E}_1|\bar{1}\rangle$, and $H_0(\mathbf{G}/2)|\bar{2}\rangle = \bar{E}_2|\bar{2}\rangle$. Thus, the general form of the two-band model of the 2×2 reduced Hamiltonian, $H^{\text{red}}(\mathbf{k})$, is expressed as

$$H^{\text{red}}(\mathbf{k}) = \begin{pmatrix} f_3 + f_0 & f_1 - if_2 \\ f_1 + if_2 & -f_3 + f_0 \end{pmatrix}$$

*E-mail: suzumura@s.phys.nagoya-u.ac.jp

$$= f_0 + f_1\sigma_1 + f_2\sigma_2 + f_3\sigma_3, \quad (4)$$

where $f_0 = (h_{11} + h_{22})/2$, $f_3 = (h_{11} - h_{22})/2$, and $f_1 - if_2 = h_{12} = f_2^*$. The quantity σ_j denotes the Pauli matrix and the coefficient $f_j (= f_j(\mathbf{k}))$ is given as the function of \mathbf{k} . Although the term f_0 gives the tilting of the Dirac cone, f_0 is irrelevant to \mathbf{B} and is discarded hereafter. Substituting Eq. (4) into Eq. (2b), we obtain the Berry curvature as¹⁶⁾

$$\mathbf{B}(\mathbf{k}) = -\frac{1}{2E^3} (f_3(\nabla_{\mathbf{k}}f_1 \times \nabla_{\mathbf{k}}f_2) + f_1(\nabla_{\mathbf{k}}f_2 \times \nabla_{\mathbf{k}}f_3) + f_2(\nabla_{\mathbf{k}}f_3 \times \nabla_{\mathbf{k}}f_1)), \quad (5)$$

where $E = \sqrt{f_1^2 + f_2^2 + f_3^2}$.

Here we mention a relation between the direction of the nodal line and that of the Berry curvature for a choice of constant $f_1(\mathbf{k})$, which is examined in the present paper. Since the Dirac nodal line consisting of Dirac point \mathbf{k}_0 is obtained by the intersection of two kinds of planes,

$$f_2(\mathbf{k}) = 0, \quad \text{and} \quad f_3(\mathbf{k}) = 0, \quad (6)$$

the direction of the line is perpendicular to both $\nabla_{\mathbf{k}}f_2(\mathbf{k})$ and $\nabla_{\mathbf{k}}f_3(\mathbf{k})$, i.e., $\nabla_{\mathbf{k}}f_2(\mathbf{k}) \times \nabla_{\mathbf{k}}f_3(\mathbf{k})$ at $\mathbf{k} = \mathbf{k}_0$. From Eq. (5), we obtain $\mathbf{B}(\mathbf{k}) \propto \nabla_{\mathbf{k}}f_2(\mathbf{k}) \times \nabla_{\mathbf{k}}f_3(\mathbf{k})$ with $\mathbf{k} = \mathbf{k}_0$. Thus, the direction of $\mathbf{B}(\mathbf{k})$ is either parallel or antiparallel to the tangent of the line and is determined by the model as shown below.

In order to understand the basic behavior of the nodal line, we first show the Berry curvature for CaAgP,⁹⁾ which consists of P_z and S orbitals with different parity. The corresponding two-band model is given by $f_2 = k_z$, $f_3 = C_0 + C_1k_z^2 + C_2(k_x^2 + k_y^2)$, ($C_0 > 0, C_1, C_2 < 0$), and $f_1 = -\Delta$, where small $\Delta (> 0)$ is introduced to obtain finite $\mathbf{B}(\mathbf{k})$. The energy is given by $\pm E$ where

$$E = \sqrt{\Delta^2 + (vk_z)^2 + (C_0 + C_1k_z^2 + C_2(k_x^2 + k_y^2))^2}. \quad (7)$$

From $f_2(\mathbf{k}_0) = f_3(\mathbf{k}_0) = 0$, the nodal line on the coplanar plane of $k_z = 0$ is obtained as $\mathbf{k}_0 = (k_0 \cos \theta, k_0 \sin \theta, 0)$ with $k_0 = \sqrt{|C_0/C_2|}$, which is in the k_x - k_y plane. Substituting this f_j 's into Eq. (5), $\mathbf{B}(\mathbf{k})$ is calculated as

$$\begin{aligned} \mathbf{B}(\mathbf{k}) &= \frac{\Delta}{2E^2} [(0, 0, v) \times (-2|C_2|k_x, -2|C_2|k_y, 2C_1k_z)] \\ &= \frac{v|C_2|\Delta}{E^{3/2}} (k_y, -k_x, 0) = |\mathbf{B}(\mathbf{k})|\vec{e}_\perp, \end{aligned} \quad (8)$$

where $\vec{e}_\perp = (\sin \theta, -\cos \theta, 0)$. It is found that $\mathbf{B}(\mathbf{k})$ is also in the k_x - k_y plane and $\mathbf{k}_0 \cdot \mathbf{B}(\mathbf{k}) = 0$. By introducing $\delta\mathbf{k} = \mathbf{k} - \mathbf{k}_0 = (\rho \cos \theta, \rho \sin \theta, k_z)$, the Berry phase γ , which is obtained from two-dimensional integral perpendicular to \vec{e}_\perp , is calculated as

$$\gamma(\mathbf{k}_0) = \int_{-\infty}^{\infty} dk_z \int_{-\infty}^{\infty} d\rho \mathbf{B} \cdot \vec{e}_\perp = \pi. \quad (9)$$

Thus the Berry phase with π exists along the nodal line, in which the odd parity of $f_2(k_z)$ is crucial.

Now we examine the nodal line of $[\text{Pd}(\text{dddt})_2]^{5)}$ consisting of two layers and 8 molecular orbitals in the unit cell with a base of 4 HOMO's ($|H1\rangle, |H2\rangle, |H3\rangle, |H4\rangle$) and 4 LUMO's ($|L1\rangle, |L2\rangle, |L3\rangle, |L4\rangle$) where HOMO (highest occupied molecular orbital) and

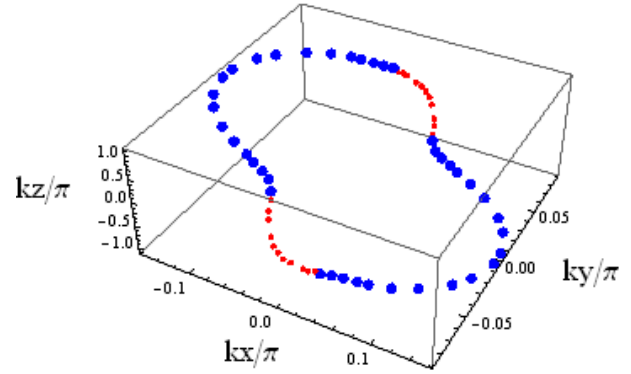


Fig. 1. (Color online) Nodal line of Dirac point at $P = 8.0$ GPa in an extended Brillouin zone, which is obtained from the original 8×8 Hamiltonian.⁶⁾ The chemical potential ($\mu = 0.5561$ eV) exists at four Dirac points $\mathbf{k}_0/\pi = \pm(-0.024, \pm 0.071, 0.65)$, which are located between the large and small symbols corresponding to $\delta E > 0$ and $\delta E < 0$ with $\delta E = E_d(\mathbf{k}_0) - \mu$.¹⁷⁾ The energy variation on the nodal is given by -0.0021 eV $< \delta E < 0.0008$ eV and $\delta E = 0$ on the chemical potential.

LUMO (lowest unoccupied molecular orbital) have different parities each other. The Dirac point is calculated by numerical diagonalization of the 8×8 tight-binding Hamiltonian,⁶⁾ where $H = H_0 + H_1$, $H_0 = H^{\text{HH}} + H^{\text{LL}}$, (H^{HH} separated from H^{LL}) and $H_1 = H^{\text{HL}}$, (coupling between HOMO and LUMO). The transfer energies between nearest-neighbor molecules are given by the interlayer (z direction) and intralayer (x - y plane) contributions. The matrix element is complex when the same phase is taken for sites in the unit cell. Multiplying the base of both HOMO and LUMO by a factor $(1, e^{-i(k_x+k_y+k_z)/2}, e^{-i(k_x+k_y)/2}, e^{-i(k_z)/2})$,⁶⁾ we obtain H_0 being real and even function with respect to \mathbf{k} and that of H_1 being pure imaginary and odd function with respect to \mathbf{k} . In Fig. 1, the Dirac nodal line in an extended Brillouin zone is shown in three-dimensional \mathbf{k} space.^{6,17)} The nodal line, which is elongated along the k_z direction and symmetric with respect to $k_y = 0$, touches the zone boundary at $k_z = \pm\pi$. It should be noted that the surface enclosed by the loop is not coplanar since typical Dirac points of $\mathbf{k}_0/\pi = (0, \pm 0.0875, 0)$ (I), $(\mp 0.015, 0, \pm 0.908)$ (II), and $\pm(-0.085, \pm 0.053, 1)$ (zone boundary) are not on the same plane. The chemical potential existing at the Dirac point between the large and small symbols suggests semimetallic state, which gives rise to a large response of the Dirac electron to the external field. Moreover large anisotropy of the Dirac cone,⁶⁾ which rotates along the nodal line also gives variety of transport measurements.

In order to examine analytically the Berry phase, we use Eqs. (3) and (4) where $f_2(\mathbf{k}) = -f_2(-\mathbf{k})$, $f_3(\mathbf{k}) = f_3(-\mathbf{k})$, and $f_1(\mathbf{k}) = -\Delta (\rightarrow -0)$. The Dirac points are symmetric with respect to $\Gamma [= (0,0,0)]$ point and also a plane of $k_y = 0$. The Dirac points of Figs. 2(a) and 2(b), which are projected from Fig. 1, show difference in magnitude compared with those obtained from Eq. (6), where $f_j(\mathbf{k})$ is calculated by perturbational method. The

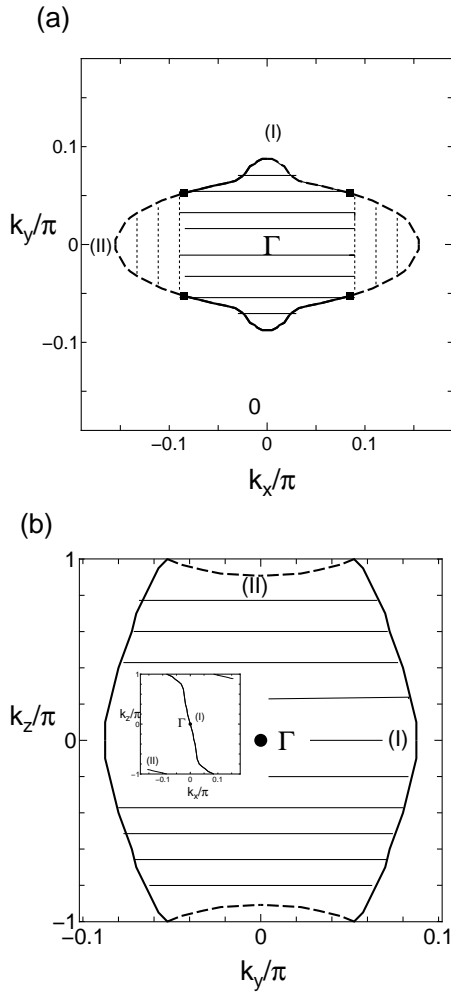


Fig. 2. Nodal line of Dirac point (solid and dashed lines) in the reduced Brillouin zone corresponding to Fig. 1, which is projected on the k_x - k_y plane (a) and on the k_y - k_z plane (b). Typical Dirac points are shown for $\mathbf{k}_0/\pi = (0, 0.0875, 0)$ (I) and $(-0.15, 0, 0.908)$ (II). The closed square in (a) corresponds to Dirac point at the zone boundary given by $\mathbf{k} = \pm(-0.085, \pm 0.0525, 1)$. The closed circle in (b) denotes Γ point. The shaded areas in (a) and (b) represent the Zak phase with $\pm\pi$, calculated from Eqs. (14a) and (14b), respectively, where the dotted line comes from the reduced zone. The inset in (b) denotes the nodal line on the k_x - k_z plane where two lines degenerate due to symmetry with respect to $k_y = 0$.

nodal line similar to Figs. 2(a) and 2(b) could be obtained by regarding $f_j(\mathbf{k})$ as a renormalized one with keeping the parity, which comes from higher order in perturbation as was usually treated.^{6,9)} Thus we examine the topological property of the Berry phase using the analytical treatment of such two-band model. Since the nodal line is complicated, we mainly examine two cases with Dirac points given by $\mathbf{k}_0/\pi = (0, \pm 0.0875, 0)$ (I), and $\mathbf{k}_0/\pi = \pm(-0.015, 0, 0.908)$, (II) and the case being slightly away from (I), i.e., $\mathbf{k}_0/\pi \simeq (0, \pm 0.0875, 0)$ (III).

For the case (I), the reduced model on the basis of TRIM at the Γ point is given by $f_2 = -C_1 k_x$, $f_3 = C - C_2 k_x^2 - C_3 k_y^2$, ($C, C_1, C_2, C_3 > 0$), $f_1 = -\Delta$, and $k_z = 0$. In this case, $\mathbf{k}_0 = (0, k_{0y}, 0)$ with $k_{0y} = (C/C_2)^{1/2}$. Expanding $k_y = k_{0y} + \delta k_y$, $\mathbf{B}(\mathbf{k})$ close to \mathbf{k}_0 is calculated

as

$$\mathbf{B}_I(\mathbf{k}) = \frac{C_1 C_3 k_{0y} \Delta}{(\Delta^2 + (C_1 k_x)^2 + (2C_3 k_{0y} \delta k_y)^2)^{3/2}} \vec{e}_z \quad (10)$$

where $\vec{e}_z = (0, 0, 1)$ and $\mathbf{B}_I(\mathbf{k})$ is perpendicular to the k_x - k_y plane. The Berry phase γ obtained from two-dimensional integral perpendicular to \vec{e}_z is calculated as

$$\gamma(\mathbf{k}_0) = \int_{-\infty}^{\infty} d k_x \int_{-\infty}^{\infty} d k_y \mathbf{B}_I \cdot \vec{e}_z = \pi k_{0y} / |k_{0y}|, \quad (11)$$

which gives $\pm\pi$.

For the case (II), the reduced model around the Z [$= (0, 0, \pi)$] point is given by $f_2 = -C_1 \tilde{k}_z$, $f_3 = C + C_2 (\tilde{k}_z)^2 - C_3 \tilde{k}_x^2$, ($C, C_1, C_2, C_3 > 0$), and $f_1 = -\Delta$ where $k_y = 0$ and $\tilde{k}_z = k_z + \text{sgn}(k_x)\pi - 0.16k_x$. In this case, $\mathbf{k}_0 = (k_{0x}, 0, k_{0z})$ with $k_{0x} = \pm(C/C_3)^{1/2}$. Expanding $k_x = k_{0x} + \tilde{k}_x$, $\mathbf{B}_{II}(\mathbf{k})$ close to \mathbf{k}_0 is calculated as

$$\mathbf{B}_{II}(\mathbf{k}) = \frac{C_1 C_3 k_{0x} \Delta}{(\Delta^2 + (C_1 (\tilde{k}_z - k_{0z}))^2 + (2C_3 \tilde{k}_x)^2)^{3/2}} \vec{e}_y, \quad (12)$$

where $\vec{e}_y = (0, 1, 0)$, and $\mathbf{B}_{II}(\mathbf{k})$ is perpendicular to the k_z - k_x plane. The Berry phase γ , which is obtained from two-dimensional integral perpendicular to \vec{e}_y , is calculated as

$$\gamma(\mathbf{k}_0) = \int_{-\infty}^{\infty} d \tilde{k}_x \int_{-\infty}^{\infty} d \tilde{k}_z \mathbf{B}_{II} \cdot \vec{e}_y = \pi k_{0x} / |k_{0x}|, \quad (13)$$

showing $\pm\pi$.

Further, we examine the Berry curvature for the case (III), which is slightly away from the case (I). Our perturbational calculation⁶⁾ gives $f_2 = -C_1 k_x - C_y k_y^2 k_z$, ($C_1, C_y > 0$), $f_3 = C - C_2 k_x^2 - C_3 k_y^2$, ($C, C_2, C_3 > 0$), and $f_1 = -\Delta$ where $\mathbf{k}_0 = (k_{0x}, k_{0y}, k_z)$ with $k_{0x} \simeq -k_z(C_y C / C_1 C_3)$ and $k_{0y} \simeq (C / C_3)^{1/2}$ for small k_z . Such Dirac point corresponds to the accidental degeneracy since the line given by $f_2(\mathbf{k}) = 0$ is irrelevant to the crystal symmetry. The Berry curvature close to $\mathbf{k} = \mathbf{k}_0$ is obtained as $\mathbf{B}_{III}(\mathbf{k}) \propto (-C_3 C_y (k_{0y})^3, C_2 C_y k_{0x} (k_{0y})^2, C_1 C_3 k_{0y} - 2C_2 C_y k_{0x} k_{0y} k_z)$. Note that $\mathbf{B}_{III}(\mathbf{k})$ at $\mathbf{k}_0 = (0, k_{0y}, 0)$ still has finite component along k_x being consistent with the direction of the nodal line at $\mathbf{k}_0 = (0, k_{0y}, 0)$. However Eq. (11) still holds since the total flux of $\mathbf{B}_{III}(\mathbf{k})$ on the k_x - k_y plane is the same as that of $\mathbf{B}_I(\mathbf{k})$. These results suggest $\gamma = \pm\pi$ for arbitrary \mathbf{k}_0 on the line, which is obtained by substituting $E = \sqrt{\Delta^2 + (\nabla_{\mathbf{k}} f_2 \cdot \delta \mathbf{k})^2 + (\nabla_{\mathbf{k}} f_3 \cdot \delta \mathbf{k})^2}$ into Eqs. (5) and (2a) with $\delta \mathbf{k} = \mathbf{k} - \mathbf{k}_0$ being perpendicular to the nodal line. Thus, it is expected that the Berry phase rotates along the nodal line anti-clockwise around the k_z axis in Fig. 1.

Here we show the Berry phase obtained from another point of view, which is known as the Zak phase. The Zak phase was originally obtained for one-dimensional periodic band.¹⁸⁾ In the present three-dimensional band, such an idea is extended by choosing a line connecting two points of $(k_x, k_y, -\pi)$ and (k_x, k_y, π) , which have the same wavefunction due to $H(k_x, k_y, -\pi) = H(k_x, k_y, \pi)$. Noting that the Dirac point or nodal line exists for the product of the parity with all the TRIM's being -1 ,¹⁹⁾ the equivalence of the Zak phase and the Berry phase is

shown as follows.²⁰⁾ When the parity of the Γ point is different from (the same as) that of the Z point, the line integral of the Berry connection between $(0, 0, -\pi)$ and $(0, 0, \pi)$ gives $\pm\pi$ (0) due to the inversion symmetry.²⁰⁾ Then, for a closed path connecting 4 points given by $(0, 0, -\pi)$ (A), $(0, 0, \pi)$ (B), $(\pi, 0, \pi)$ (C), and $(\pi, 0, -\pi)$ (D), one finds that the line integral gives $\pm\pi$ for AB, 0 for BC+DA due to the zone boundary, and 0 for CD due to both C and D having the same parity as X $(\pi, 0, 0)$. Therefore the Zak phase given by AB is equal to the Berry phase given by ABCD. Based on this argument, we obtain the Zak phase with $\pm\pi$ when the line with arbitrary $(k_x, k_y \pm \pi)$ exists in the area including the Γ point. Thus, in terms of the Berry connection, these phases can be written explicitly as

$$\gamma_z(k_x, k_y) = i \int_{-\pi}^{\pi} dk_z \langle n(\mathbf{k}) | \nabla_{k_z} | n(\mathbf{k}) \rangle, \quad (14a)$$

$$\gamma_x(k_y, k_z) = i \int_{-\pi}^{\pi} dk_x \langle n(\mathbf{k}) | \nabla_{k_x} | n(\mathbf{k}) \rangle, \quad (14b)$$

which are line integrals along a straight path connecting two points of $(k_x, k_y, \pm\pi)$ and $(\pm\pi, k_y, k_z)$ for $\gamma_z(k_x, k_y)$ and $\gamma_x(k_y, k_z)$, respectively. In Figs. 2(a) and 2(b), the Zak phase becomes $\pm\pi$ in the region including the Γ point (shaded area) and zero outside. The dashed line comes from a nodal line of the extended zone. As shown in the inset of Fig. 2(b), there is no area for $\gamma_y(k_z, k_x) = \pi$ due to the inversion symmetry of the band with respect to $k_y = 0$. There are common features between these two Zak phases since the parity of the Γ point is different from the other TRIM's, e.g., Z and X points.⁶⁾

We comment on the recent paper by Liu *et al.*,²¹⁾ who obtained the nodal line of $[\text{Pd}(\text{dddt})_2]$ using the same crystal data as ref. 5. Their two-band Hamiltonian, where the coefficients $g_1(\mathbf{k})$ and $g_3(\mathbf{k})$ correspond to our $f_2(\mathbf{k})$ and $f_3(\mathbf{k})$, respectively, also gives the Berry curvature by adding a small potential to $g_2(\mathbf{k}) \rightarrow \Delta$, which is clear from Eq. (5). The nodal line in ref. 21 is located close to the Γ point while that of the tight-binding model⁶⁾ exists in the extended zone. Such geometry of the nodal line is also obtained in the previous DFT calculation,²²⁾ where a pair of Dirac points appear at the fractional coordinates of $\mathbf{k}_0/2\pi = (0.0, \pm 0.085, 0.0)$ along the Γ -Y direction and the loop extends to those of $(-0.1960, 0.000, \pm 0.3875)$ in the $k_x - k_z$ plane. This shows a difference between the DFT calculation and the tight-binding model based on the extended Hückel calculation. Further the DFT calculation shows a clear evidence of the non-coplanar nodal line, e.g., a Dirac point $\mathbf{k}_0/2\pi = (-0.1310, \pm 0.0570, 0.200)$ is located away from the same plane.²²⁾ This non-coplanar behavior, which shares a common feature with the tight-binding mode,⁶⁾ indicates the most complicated origin of the accidental degeneracy.¹⁾ Note that Eq. (14a) is equal to the Wannier charge center in ref. 21, which is obtained by the

summation of all the occupied bands.

Finally we discuss the possible experiment on the nodal line through the Berry phase. The Landau level ($\propto \sqrt{nB}$) (n being an integer) relevant to the Dirac cone of Fig. 1 is expected for all the directions due to the loop and large anisotropy.¹⁵⁾ There is also a suggestion for the surface charge polarization in the nodal line semimetal,²³⁾ which is proportional to the area of the Zak phase, S_{Zak} . From the shaded region in Fig. 2(a) and 2(b), the ratio of S_{Zak} to that of each Brillouin zone in the present case is given by $\simeq 0.01$ and 0.06 , respectively.

In summary, we examined the Berry phase associated with the Dirac nodal line of $[\text{Pd}(\text{dddt})_2]$, where the almost temperature-independent resistivity was observed. The present nodal line with the three-dimensional loop provides the Berry curvature and the Zak phase essentially given by $\gamma_x(k_y, k_z)$, which is compatible with the direction of the conductivity showing the typical property of the Dirac electrons.¹⁵⁾

Acknowledgements

One of the authors (Y.S.) thanks R. Kato and T. Tsumuraya for useful discussions on the Dirac nodal line of $[\text{Pd}(\text{dddt})_2]$.

- 1) C. Herring, Phys. Rev. **52**, 365 (1937).
- 2) J. W. McClure, Phys. Rev. **104**, 666 (1956).
- 3) K. S. Novoselov, A. K. Geim, S. V. Morozov, D. Jiang, M. I. Katsnelson, I. V. Grigorieva, S. V. Dubonos, and A. A. Firsov, Nature **438**, 197 (2005).
- 4) S. Katayama, A. Kobayashi, and Y. Suzumura, J. Phys. Soc. Jpn. **75**, 054705 (2006).
- 5) R. Kato, H.B. Cui, T. Tsumuraya, T. Miyazaki, and Y. Suzumura, J. Am. Chem. Soc. **139**, 1770 (2017).
- 6) R. Kato and Y. Suzumura, J. Phys. Soc. Jpn. **86**, 064705 (2017).
- 7) S. Murakami, New J. Phys. **9**, 356 (2007).
- 8) A.A. Burkov, M.D. Hook, and L. Balents, Phys. Rev. B **84**, 235126 (2011).
- 9) A. Yamakage, Y. Yamakawa, Y. Tanaka, and Y. Okamoto J. Phys. Soc. Jpn. **85**, 013708 (2016).
- 10) C. Fang, H. Weng, X. Dai, and Z. Fang, Chinese Physics B **25**, 117106 (2016).
- 11) S.-Y. Yang, H. Yang, E. Derunova, Stuart S. P. Parkin, B. Yan, and Mazhar N. Ali, Advances in Physics, X **3**, 1414631 (2018).
- 12) M. Hirayama, R. Okugawa, and S. Murakami, J. Phys. Soc. Jpn. **87**, 041002 (2018).
- 13) A. Bernevig, H. Weng, Z. Fang, and X. Dai, J. Phys. Soc. Jpn. **87**, 041001 (2018).
- 14) M. V. Berry: Proc. R. Soc. Lond. A **392**, 45 (1984).
- 15) Y. Suzumura, H.B. Cui, and R. Kato, J. Phys. Soc. Jpn. **87**, 084702 (2018).
- 16) Y. Suzumura and A. Kobayashi, J. Phys. Soc. Jpn. **80**, 104701 (2011).
- 17) Y. Suzumura, J. Phys. Soc. Jpn. **86**, 124710 (2017).
- 18) J. Zak, Phys. Rev. Lett. **62**, 2747 (1988).
- 19) L. Fu and C. L. Kane, Phys. Rev. B **76**, 045302 (2007).
- 20) Y. Kim, B. J. Wieder, C. L. Kane, and A. M. Rappe, Phys. Rev. Lett. **115**, 036806 (2015); and the supplement.
- 21) Z. Liu, H. Wang, Z. F. Wang, J. Yang, and F. Liu, Phys. Rev. B **97**, 155138 (2018).
- 22) T. Tsumuraya, H. Sawahata, F. Ishii, H. Kino, R. Kato, T. Miyazaki, Am. Phys. Soc. Bull., R14.00012 (2018).
- 23) M. Hirayama, R. Okugawa, T. Miyake, S. Murakami, Nature Communications **8**, 14022 (2017).